Subspace Leakage in Conventional and Dimensionally Spread Null-Space Communications

Jordi Borras, *Member, IEEE*, and Gregori Vazquez, *Senior Member, IEEE*

***Abstract*—This letter evaluates the impact of subspace leakage in conventional (single-dimension) and dimensionally spread null-space precoding schemes. This phenomenon arises when the null-space inference procedure lacks precision and suffers subspace detection errors. The analysis relies on the signal-to-interference-per-dimension ratio (SIDR) metric, which jointly measures the transmitted power efficiency and the interference-mitigation robustness of the adopted transmission scheme. Based on theoretical and numerical analyses of the SIDR, this letter provides the explicit SIDR performance gain of dimension spreading-based null-space precoding schemes as an interference mitigation strategy in front of conventional approaches.**

***Index Terms*—Null-space precoding, opportunistic interference alignment, subspace leakage, interference networks.**

I. Introduction

NULL-SPACE PRECODING is a class of transmission formats that permit mitigating –ideally avoiding– interferences by steering the transmitted symbols through the null space of other users [1–12]. The precoder design relies on the inference of the null space, which typically involves a subspace detection scheme on an estimated statistic; thus, the null-space inference procedure almost surely suffers from subspace detection errors. Specifically, some of the signal-space dimensions used/occupied by other users are erroneously detected as unused or available. This phenomenon, known as *subspace leakage* [13], decreases the interference-mitigation efficiency of null-space precoding techniques, inducing harmful interferences on other users. Motivated by the lack of robustness exhibited by conventional or single-dimension (SD) null-space precoding schemes, the authors studied in [14] a generalized approach based on dimension spreading (DS), giving birth to a class of π-waveforms (*Projection-Invariant* waveforms), that minimizes the impact of subspace leakage.

Complementing [14], this letter analyzes the critical impact of subspace leakage on both SD and DS null-space precoding strategies. While related works on this topic focus the analysis on modeling the estimation errors of the statistic for subspace detection [1], [8] or on the pessimistic null-space swap [15], the reported analysis relies on the so-called signal-to-interference-per-dimension ratio (SIDR) metric. This metric, which was previously used by the authors in [14], measures the ratio between the transmitted non-interfering power and the transmitted interference power per erroneously sensed null-space dimension or degree of freedom (DoF). Since this metric is measured at the transmitter output, the analysis is independent of both small-scale and large-scale fading coefficients, the wireless network topology, and the coded-modulation formats adopted by coexisting users. Note that, by definition, the SIDR permits jointly evaluating the robustness of the adopted null-space precoding scheme to the two main effects of subspace leakage: the undesired interferences induced on non-intended receivers and the power loss in the intended communication.

Based on the adopted framework, this letter theoretically and numerically quantifies the impact of subspace leakage on SD and DS null-space precoding schemes as a function of the given operating conditions; thus, providing a general enough framework to evaluate the worst-case operating regimes. In particular, the derived closed-form expressions permit evaluating the influence of the total number of signal-space dimensions or DoF N, the null-space detection inaccuracy ϵ, the detected DoF availability μ, and the null-space utilization factor κ on the worst-case performance. Moreover, this letter also provides the performance superiority of DS in front of SD strategies. In this sense, it is found that the average SIDR exhibited by DS schemes is $N\mu\epsilon$ times larger than the average SIDR of SD strategies; under worst-case conditions, this performance gain enlarges to $N\mu\epsilon\frac{1-\epsilon}{\kappa-\epsilon}$, highlighting the expected superiority of DS schemes under subspace leakage.

II. Model

Without loss of generality, consider the scenario depicted in Figure 1, where a vector of K zero-mean and unit-variance independent symbols $\boldsymbol{s} \in \mathbb{C}^K$ has to be transmitted through the channel $\boldsymbol{H}$. To mitigate –ideally, avoid– the interference induced on the non-intended receiver(s), a null-space precoding format is employed such that the transmitted signal[1] yields $\boldsymbol{x} = \boldsymbol{\Phi}\boldsymbol{s}$, where $\boldsymbol{\Phi} \triangleq [\phi_0, \ldots, \phi_{K-1}]$ is the null-space precoding matrix, satisfying the interference-free condition:

$$\boldsymbol{W}^H \boldsymbol{G}\boldsymbol{\Phi} = \boldsymbol{0}, \tag{1}$$

being $\boldsymbol{G}$ the interference-channel matrix and $\boldsymbol{W}$ the combining matrix used by the non-intended receiver(s)[2]. $(\cdot)^H$ denotes the

This work has been supported by the Spanish Ministry of Science and Innovation through project RODIN (PID2019-105717RB-C22 / MCIN / AEI / 10.13039/501100011033) and fellowship FPI BES-2017-080071.

J. Borras was with the Department of Signal Theory and Communications of the Technical University of Catalonia (UPC), 08034 Barcelona, Spain. He is now with the atlanTTic Research Center, University of Vigo, 36310 Vigo, Spain. G. Vazquez is with the Department of Signal Theory and Communications of the Technical University of Catalonia (UPC), 08034 Barcelona, Spain. E-mail: jordi.borras@ieee.org, gregori.vazquez@upc.edu

[1]Additional processing can be employed to deal with the intended channel $\boldsymbol{H}$ and improve the spectral efficiency, yet omitted in this letter for simplicity.

[2]Despite only one non-intended receiver is depicted in Figure 1, the extension to the case of Q non-intended receivers is implicit by defining $\boldsymbol{G} \triangleq [\boldsymbol{G}_1^H \cdots \boldsymbol{G}_Q^H]^H$ and $\boldsymbol{W} \triangleq [\boldsymbol{W}_1^H \cdots \boldsymbol{W}_Q^H]^H$, being $\boldsymbol{G}_q$ the interference-channel matrix between TX #1 and the non-intended receiver q and $\boldsymbol{W}_q$ the combining matrix at the q-th non-intended receiver.

 DOI 10.1109/LCOMM.2023.3306432

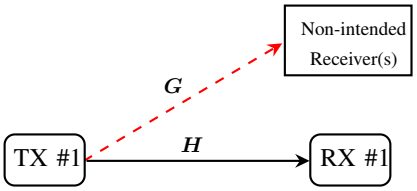

Fig. 1. Generic system model for null space-based communication. The dimensions of the channel matrices $\boldsymbol{H}$ and $\boldsymbol{G}$ are not given for the sake of generality, as this formulation is valid for both single- and multi-antenna scenarios under both narrowband and wideband conditions.

transpose conjugate (Hermitian) operator. Note that (1) can be satisfied when the null-space precoding matrix $\boldsymbol{\Phi}$ lies in the null space of the interference-channel matrix $\boldsymbol{G}$, given by $\mathcal{N}(\boldsymbol{G}) \triangleq \{\boldsymbol{z} : \boldsymbol{G}\boldsymbol{z} = \boldsymbol{0},\ \boldsymbol{z} \neq \boldsymbol{0}\}$, which is the operating principle of zero-forcing precoding [1–7]. A more sophisticated strategy consists in designing the null-space precoding matrix $\boldsymbol{\Phi}$ to lie in the null space of the matrix $\boldsymbol{G}_{\text{eff}} = \boldsymbol{W}^H\boldsymbol{G}$. The latter is the operating principle of the so-called OIA schemes [8–11]. Note that the former case can be seen as a particular case of the latter; nevertheless, the OIA approach tends to exploit a larger null space, as $\mathcal{N}(\boldsymbol{G}) \subseteq \mathcal{N}(\boldsymbol{G}_{\text{eff}})$.

Either way, satisfying (1) requires TX #1 to know the interference-channel matrix $\boldsymbol{G}$, which can be learned through a channel estimation scheme, and/or the combining matrix $\boldsymbol{W}$, which can be conveyed through feedback from the non-intended receiver(s). Under channel reciprocity, it is also possible to directly estimate the effective interference-channel matrix $\boldsymbol{G}_{\text{eff}}$. In both cases, the considered statistic for inferring the null space is sensitive to the time variability of the channel and the network conditions. This sensitivity also hinders the required feedback to convey the needed side information.

Another alternative, which is robust to the time variability and does not rely on cooperative feedback, is to estimate the second-order statistics of the interference that TX #1 sees from the interference channel $\boldsymbol{G}$. Without loss of generality[3], we consider in the sequel that the null space is inferred from the autocorrelation matrix.

A. Generalized Null-Space Error Model

In practice, the interference autocorrelation matrix has to be estimated from a set of measurements $\mathcal{M} = \{\boldsymbol{s}_q\}_{0\leq q\leq Q-1}$. The conventional sample estimate $\widehat{\boldsymbol{R}} = 1/Q\sum_q \boldsymbol{s}_q\boldsymbol{s}_q^H \in \mathbb{C}^{N\times N}$ is a *sufficient statistic* for finding the signal (or null) subspace in the least-squares sense. The magnitude N refers to the total number of signal-space dimensions, and it is commonly known as degrees of freedom (DoF) [16]. It is worth noting that, in single-antenna scenarios, the total number of complex DoF is approximated by the time-bandwidth product, i.e., $N \approx TW$. The use of $L > 1$ antennas can increase the total number of complex DoF to $N \approx \eta TW$, where $\eta \leq L$ and the equality holds if the L antennas are statistically independent. As in [14], the case $L = 1$ is considered in the sequel.

[3]The approach based on the autocorrelation matrix adopted in this letter is general enough for the subsequent technical discussion. If the null space is inferred from the interference channel matrix $\boldsymbol{G}$ (or $\boldsymbol{G}_{\text{eff}}$), a unitary basis of the null space can be obtained from the right-singular vectors matrix, which corresponds to the eigenvectors' matrix of $\boldsymbol{G}^H\boldsymbol{G}$ (or $\boldsymbol{G}_{\text{eff}}^H\boldsymbol{G}_{\text{eff}}$).

Consider the *eigendecomposition* of the sample estimate interference autocorrelation matrix $\widehat{\boldsymbol{R}} = \widehat{\boldsymbol{U}}\widehat{\boldsymbol{D}}\widehat{\boldsymbol{U}}^H$, where $\widehat{\boldsymbol{U}} \in \mathbb{C}^{N\times N}$ is a unitary matrix containing the eigenvectors and $\widehat{\boldsymbol{D}} \in \mathbb{C}^{N\times N}$ is a positive semidefinite diagonal matrix encompassing the eigenvalues sorted in non-increasing order. The null space is spanned by the M eigenvectors associated with the M least significant eigenvalues. Thus, a unitary[4] basis of the estimated null space, namely $\widehat{\boldsymbol{U}}_{\mathcal{N}}$, can be obtained by partitioning matrix $\widehat{\boldsymbol{U}}$ as $\widehat{\boldsymbol{U}} = \left[\begin{array}{c:c} \widehat{\boldsymbol{U}}_{\mathcal{S}} & \widehat{\boldsymbol{U}}_{\mathcal{N}} \end{array}\right]$, where $\widehat{\boldsymbol{U}}_{\mathcal{S}} \in \mathbb{C}^{N\times(N-M)}$ spans the *estimated signal subspace* and $\widehat{\boldsymbol{U}}_{\mathcal{N}}\in\mathbb{C}^{N\times M}$ constitutes a basis of the *estimated null space*, which is the basis of interest for designing the precoding matrix $\boldsymbol{\Phi}$, being M the dimension of the estimated null space.

The partitioning of $\widehat{\boldsymbol{U}}$, which is known as *subspace estimation* or *model order selection*, is highly critical. If the dimension of the null space M is underestimated, TX #1 loses transmission opportunities. Although the latter incurs an information-rate loss, it is not critical in terms of inducing interference. Nevertheless, if M is overestimated, TX #1 will cause interference on the non-intended receiver(s), which is critical in interference-limited applications.

For the purpose of characterizing the critical null-space inference errors, let us write the unitary basis $\widehat{\boldsymbol{U}}_{\mathcal{N}}$ as

$$\widehat{\boldsymbol{U}}_{\mathcal{N}} = \left[\begin{array}{c:c} \widetilde{\boldsymbol{U}}_{\mathcal{N}} & \boldsymbol{E}_{\mathcal{N}} \end{array}\right], \tag{2}$$

where $\widetilde{\boldsymbol{U}}_{\mathcal{N}} \in \mathbb{C}^{N\times(M-N_E)}$ contains the correctly detected null-space eigenvectors, whereas $\boldsymbol{E}_{\mathcal{N}} \in \mathbb{C}^{N\times N_E}$ models the N_E signal-subspace DoF that are erroneously included in the estimated null space. The model in (2) is transparent to TX #1, and only employed in the sequel for the technical analysis.

B. Null Space-based Precoding

Using a basis of the estimated null space, the null-space precoding matrix $\boldsymbol{\Phi} = [\boldsymbol{\phi}_0, \ldots, \boldsymbol{\phi}_{K-1}]$ can be designed as

$$\boldsymbol{\phi}_k = \widehat{\boldsymbol{U}}_{\mathcal{N}}\boldsymbol{\lambda}_k = \left[\begin{array}{c:c} \widetilde{\boldsymbol{U}}_{\mathcal{N}} & \boldsymbol{E}_{\mathcal{N}} \end{array}\right]\boldsymbol{\lambda}_k, \quad \text{for } k = 0, \ldots, K-1, \tag{3}$$

where $\boldsymbol{\lambda}_k \in \mathbb{C}^M$ is the linear combination coefficient vector that describes each column $\boldsymbol{\phi}_k$ of the precoding matrix $\boldsymbol{\Phi}$.

Depending on how the coefficient vectors $\boldsymbol{\lambda}_k$, for $k = 0, \ldots, K-1$, are designed, we can essentially distinguish two null-space precoding approaches:

1) Conventional or Single-Dimension (SD) Null-Space Precoding: This approach consists in arbitrarily selecting K null-space eigenvectors from $\widehat{\boldsymbol{U}}_{\mathcal{N}}$ as a precoding matrix; thus the coefficient vectors are given by

$$\boldsymbol{\lambda}_k^{\text{SD}} = [\boldsymbol{0}_{m(k)-1}^T\ 1\ \boldsymbol{0}_{M-m(k)}^T]^T, \quad \text{for } k = 0, \ldots, K-1, \tag{4}$$

with $m(k) \in \{1, \ldots, M\} \setminus \{m(0), \ldots, m(k-1)\}$.

[4]Even though this letter considers unitary null-space basis, the discussion is still valid if TX #1 obtains a non-unitary basis spanning the null space, a unitary basis can be obtained from its singular value decomposition, the QR decomposition, or the canonical transformation.

2) Dimension Spreading (DS) Approach: A more general strategy consists in letting the vectors $\boldsymbol{\lambda}_k$ be generic unitary full-vectors and sequentially forcing them to be orthogonal, i.e., $\boldsymbol{\lambda}_{k'}^H \boldsymbol{\lambda}_k = 0,\ k \neq k'$, in order to fully exploit the available DoF. In this sense, the π-waveforms found in [14] justify the optimality of the DS approach in terms of minimum worst-case null-space inference errors. As for in [14], the coefficient vectors defining the π-waveforms are given by

$$\boldsymbol{\lambda}_k^{\pi} = \gamma_k \widehat{\boldsymbol{U}}_{\mathcal{N}}^H \left[\boldsymbol{I}_N - \sum\nolimits_{i=0}^{k-1} \widehat{\boldsymbol{U}}_{\mathcal{N}} \boldsymbol{\lambda}_i^{\pi} (\boldsymbol{\lambda}_i^{\pi})^H \widehat{\boldsymbol{U}}_{\mathcal{N}}^H \right] \boldsymbol{e}_{n(k)}, \quad (5)$$

where γ_k is scaling factor such that $\|\boldsymbol{\lambda}_k^{\pi}\| = 1$, being $\|\cdot\|$ the vector L_2-norm, and $\boldsymbol{e}_{n(k)} = [\boldsymbol{0}_{n(k)-1}^T\ 1\ \boldsymbol{0}_{N-n(k)}^T]^T$, with $n(k) \in \{1, \ldots, N\}$, where the position $n(k)$ of the non-zero entry is chosen to satisfy the minimum worst-case interference criterion and corresponds to the index of the minimum diagonal element of $\widehat{\boldsymbol{P}}_k = \widehat{\boldsymbol{U}}_{\mathcal{N}} \widehat{\boldsymbol{U}}_{\mathcal{N}}^H \left[\boldsymbol{I}_N - \sum_{i=0}^{k-1} \widehat{\boldsymbol{U}}_{\mathcal{N}} \boldsymbol{\lambda}_i^{\pi} (\boldsymbol{\lambda}_i^{\pi})^H \widehat{\boldsymbol{U}}_{\mathcal{N}}^H \right]$, that is, the projector onto a subset of the estimated null space.

This generalized approach spreads each transmitted symbol within all M dimensions of the estimated null space while keeping the orthogonality between the columns of $\boldsymbol{\Phi}$, thus denoted as Dimension Spreading (DS). This spreading, which reduces the induced (average) interference level per dimension, does not imply losing effective dimensions as each π-waveform is rank-one. Thus, the DS approach keeps the achieved efficiency by SD solutions in asynchronous scenarios.

III. Signal-to-Interference-Per-Dimension Ratio (SIDR) Analysis

This section compares the interference mitigation capability of both null-space precoding approaches described in Section II. For this purpose, we define the Signal-to-Interference-per-Dimension Ratio (SIDR) metric as

$$\mathrm{SIDR} \triangleq \frac{S_T - I_T}{I_{\mathrm{DoF}}} = \frac{\frac{1}{N}\sum_{k=0}^{K-1} \|\boldsymbol{\phi}_k\|^2 - \frac{1}{N}\sum_{k=0}^{K-1} \left\|\boldsymbol{E}_{\mathcal{N}}^H \boldsymbol{\phi}_k\right\|^2}{I_{\mathrm{DoF}}}, \quad (6)$$

where S_T, I_T, and I_{DoF} refer to the total time-average transmitted power, the total time-average induced interference level, and the time-average induced interference level per erroneously identified dimension, respectively. Since (6) measures the ratio between the non-interfering transmitted power and the interference level per dimension, the SIDR quantifies not only the robustness to subspace leakage exhibited by a transmission scheme but also the power or energy efficiency, in the sense that the SIDR indicates the ratio between the total *useful* power and power lost per wrongly identified dimension.

Assuming $\boldsymbol{\Phi}^H \boldsymbol{\Phi} = \boldsymbol{I}_K$ without loss of generality, $S_T = K/N$. The magnitudes I_T and I_{DoF} depend on the considered null-space precoding approach and are studied in the sequel.

A. Conventional or Single-Dimension Null-Space Precoding

The precoding matrix $\boldsymbol{\Phi}$ under the SD approach is a column subset of the basis of the estimated null space.

Accordingly, since each column of matrix $\boldsymbol{\Phi}$ spans the same dimension as the corresponding column of $\widehat{\boldsymbol{U}}_{\mathcal{N}}$, we have that $I_T^{\mathrm{SD}} = I_{\mathrm{DoF}}^{\mathrm{SD}}$. Particularizing I_T in (6), I_T^{SD} reads as

$$I_T^{\mathrm{SD}} = \frac{1}{N} \sum\nolimits_{k=0}^{K-1} \|\boldsymbol{\phi}_k\|^2 \mathbb{1}_k, \quad (7)$$

where $\mathbb{1}_k$ is the conventional indicator function, that is, $\mathbb{1}_k = 1$ if $\boldsymbol{\phi}_k \in \langle \boldsymbol{E}_{\mathcal{N}} \rangle$; otherwise, $\mathbb{1}_k = 0$.

Note that the choice in $\mathbb{1}_k$ depends on the column selection, which is typically arbitrary. To remove the column selection uncertainty, recall that the mathematical expectation of $\mathbb{1}_k$ is N_E/M, which leads to an average SIDR of

$$\mathrm{SIDR}_{\mathrm{SD}}^{\mathrm{avg}} = \frac{K/N - K/N \cdot N_E/M}{K/N \cdot N_E/M} = \frac{1-\epsilon}{\epsilon}, \quad (8)$$

which is independent of the number of exploited null-space dimensions K and only depends on the null-space detection inaccuracy $\epsilon \triangleq N_E/M$.

Even though (8) provides the average performance of SD in terms of SIDR, we shall now discuss the worst-case SIDR achievable by SD schemes. To this end, we have to assume that $N_E \leq K \leq M$, implying that at least all the N_E erroneously identified null-space dimensions are selected for transmission. Under these conditions, we note that the time-average induced interference level equals $I_{T,\text{worst-case}}^{\mathrm{SD}} = N_E/N$, leading to an achievable SIDR of

$$\mathrm{SIDR}_{\mathrm{SD}}^{\text{worst-case}} = \frac{K/N - N_E/N}{N_E/N} = \frac{\kappa - \epsilon}{\epsilon}, \quad (9)$$

which is only valid for $N_E \leq K \leq M$. Note that (9) depends on the fraction of exploited null-space dimensions $\kappa \triangleq K/M$, which emphasizes the lack of robustness to null-space inference errors exhibited by SD schemes.

B. Dimension Spreading-based Null-Space Precoding

In the DS scheme case, we will focus on the π-waveforms approach. As per [14], the DS-based precoding scheme satisfies a minimum worst-case induced interference criterion; thus, the SIDR achievable by the π-waveforms approach corresponds to the worst-case SIDR. Moreover, thanks to the dimension-spreading property, we have that $I_{\mathrm{DoF}}^{\pi} = I_T^{\pi}/N_E$, where N_E is a consequence of spreading the interference over all erroneously inferred null-space dimensions.

As studied in Appendix, the total time-average induced interference level for the π-waveforms case is given by

$$I_T^{\pi} = \frac{1}{N} \sum_{k=0}^{K-1} \frac{\boldsymbol{e}_{n(k)}^T \widehat{\boldsymbol{P}}_{\mathcal{E}} \boldsymbol{e}_{n(k)} + \delta_k}{\boldsymbol{e}_{n(k)}^T \widehat{\boldsymbol{P}}_0 \boldsymbol{e}_{n(k)} + \xi_k}, \quad (10)$$

where $\widehat{\boldsymbol{P}}_0 = \widehat{\boldsymbol{U}}_{\mathcal{N}} \widehat{\boldsymbol{U}}_{\mathcal{N}}^H$ is the orthogonal projector onto the inferred null space $\langle \widehat{\boldsymbol{U}}_{\mathcal{N}} \rangle$, $\widehat{\boldsymbol{P}}_{\mathcal{E}} = \boldsymbol{E}_{\mathcal{N}} \boldsymbol{E}_{\mathcal{N}}^H$ is the orthogonal projector onto the erroneous null space $\langle \boldsymbol{E}_{\mathcal{N}} \rangle$, and δ_k and ξ_k are second-order terms containing combinations of off-diagonal elements of projectors $\widehat{\boldsymbol{P}}_0$ and/or $\widehat{\boldsymbol{P}}_{\mathcal{E}}$.

Even though it is not possible to derive a closed-form expression for I_T^{π}, this quantity can be asymptotically characterized. When N is sufficiently large and $M \gg 1$, off-diagonal elements of spectral projectors become irrelevant in comparison with diagonal elements [17]. Thus, under these conditions, $\delta_k, \xi_k \to 0$ leading to

$$I_T^{\pi} \approx \frac{1}{N} \sum_{k=0}^{K-1} \boldsymbol{e}_{n(k)}^T \widehat{\boldsymbol{P}}_{\mathcal{E}} \boldsymbol{e}_{n(k)} \left(\boldsymbol{e}_{n(k)}^T \widehat{\boldsymbol{P}}_0 \boldsymbol{e}_{n(k)} \right)^{-1}. \quad (11)$$

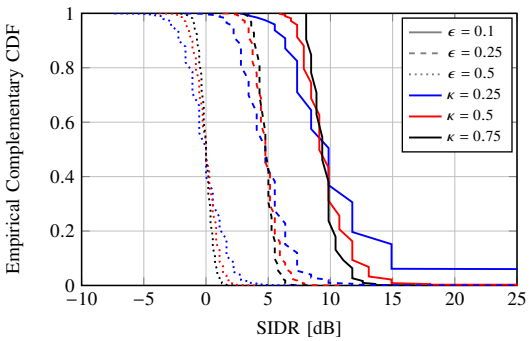

Fig. 2. Empirical complementary CDF of the SIDR exhibited by SD for different ϵ and κ evaluated over 10^6 Monte Carlo runs.

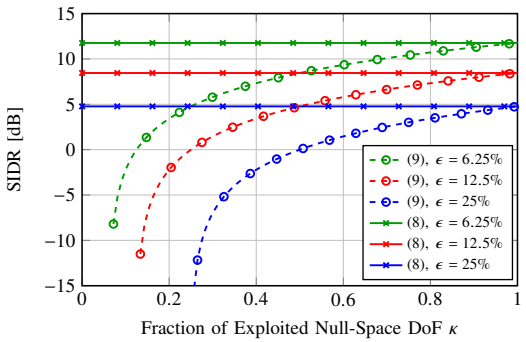

Fig. 3. Theoretical (lines) and simulated (markers) SIDR exhibited by SD as a function of κ for different ϵ.

Note that (11) depends only on diagonal elements of projectors $\widehat{\boldsymbol{P}}_0$ and $\widehat{\boldsymbol{P}}_{\mathcal{E}}$. Under wide sense stationary (WSS) conditions, when N is sufficiently large, a consequence of the Szegö's Theorem [18] states that the eigenvectors' matrix of any $N \times N$ autocorrelation matrix converge to the normalized N-size Fourier matrix, implying that $\widehat{\boldsymbol{P}}_0$ and $\widehat{\boldsymbol{P}}_{\mathcal{E}}$ will have constant diagonal elements given by $\boldsymbol{e}_{n(k)}^T \widehat{\boldsymbol{P}}_{\mathcal{E}} \boldsymbol{e}_{n(k)} = N_E/N$ and $\boldsymbol{e}_{n(k)}^T \widehat{\boldsymbol{P}}_0 \boldsymbol{e}_{n(k)} = M/N$. Consequently, the worst-case SIDR for the π-waveforms approach equals its average SIDR performance and can be approximated by

$$\mathrm{SIDR}_{\mathrm{DS}}^{\text{worst-case}} = \mathrm{SIDR}_{\mathrm{DS}}^{\text{avg}} \approx \frac{K - K\frac{N_E/N}{M/N}}{\frac{1}{N_E} K \frac{N_E/N}{M/N}} = N\mu\,(1-\epsilon)\,, \quad (12)$$

which depends on the total number of system DoF N, the relative dimension of the estimated null space $\mu \triangleq M/N$, and the null-space detection inaccuracy ϵ.

IV. Numerical Analysis and Discussion

This section provides a simulation study of the SIDR metric exhibited by both SD and DS approaches discussed so far.

The SIDR performance of SD schemes (4) depends on the arbitrariness of the considered column selection criterion. In order to illustrate the performance from a general viewpoint, the complementary cumulative distribution function (CDF) has been empirically evaluated in Figure 2. In this simulation, we have considered different null-space detection inaccuracies $\epsilon = \{0.1, 0.25, 0.5\}$ and different null-space exploitation levels $\kappa = \{0.25, 0.5, 0.75\}$. Even though different numbers of total signal-space dimensions or DoF N and different relative dimensionality of the null-space μ have been tested, no significant differences were observed. As predicted by (8), the parameter ϵ introduces a worsening in the average performance. Concerning the parameter κ, which somehow controls the achievable information rate, as it increases the achievable SIDR converges to the average behavior.

The worst case discussed in Section III-A, which implies that $K \geq N_E$ and that the N_E erroneous dimensions are exploited for transmission, is evaluated in Figure 3. The numerical evaluation confirms that the average SIDR is independent of the null-space exploitation level κ, and that, under worst-case conditions, the null space must be fully exploited to achieve the average performance.

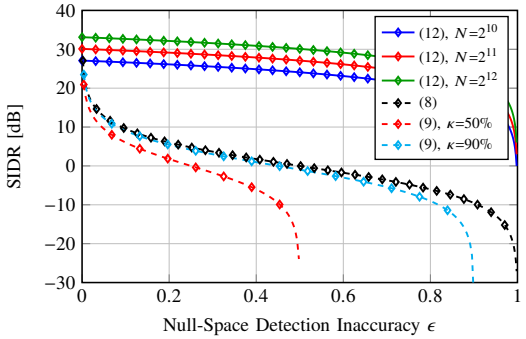

Fig. 4. Theoretical (lines) and simulated (markers) SIDR exhibited by SD and DS approaches for $\mu = 0.25$ and different values of N and κ.

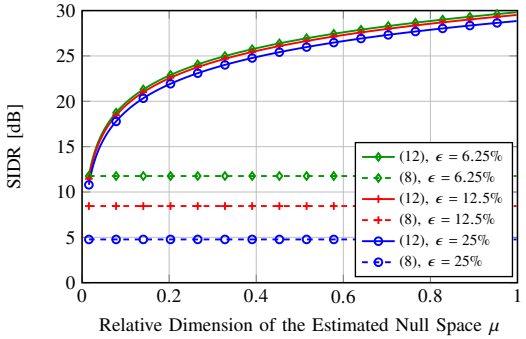

Fig. 5. Theoretical (lines) and simulated (markers) SIDR exhibited by SD and DS approaches for $N = 2^{10}$ and different values of ϵ.

Since the SIDR of the DS-based null-space precoding does not depend on any arbitrary criteria as all dimensions of the estimated null space are optimally combined to minimize the interference induced by null-space inference errors, we compare in Figures 4 and 5 the simulated and theoretical SIDR exhibited by SD and π-waveforms schemes as a function of ϵ and μ, respectively. Note that the π-waveforms approach, which provides the minimum worst-case induced interferences in the DS case, clearly outperforms SD schemes in terms of SIDR. In fact, it follows from (8) and (12) that

$$\frac{\mathrm{SIDR}_{\mathrm{SD}}^{\text{avg}}}{\mathrm{SIDR}_{\mathrm{DS}}^{\text{avg}}} = \frac{1}{N\mu\epsilon}. \quad (13)$$

Since $N\mu\epsilon = N_E$, this factor can be seen as a performance gain

$$\boldsymbol{e}_{n(k)}^T\widehat{\boldsymbol{P}}_k\widehat{\boldsymbol{P}}_{\mathcal{E}}\widehat{\boldsymbol{P}}_k\boldsymbol{e}_{n(k)} = \boldsymbol{e}_{n(k)}^T\widehat{\boldsymbol{P}}_0\left(\boldsymbol{I}_N - \sum_{i=0}^{k-1}\boldsymbol{\phi}_i^{\pi}(\boldsymbol{\phi}_i^{\pi})^H\right)\widehat{\boldsymbol{P}}_{\mathcal{E}}\widehat{\boldsymbol{P}}_0\left(\boldsymbol{I}_N - \sum_{i=0}^{k-1}\boldsymbol{\phi}_i^{\pi}(\boldsymbol{\phi}_i^{\pi})^H\right)\boldsymbol{e}_{n(k)}$$
$$= \boldsymbol{e}_{n(k)}^T\widehat{\boldsymbol{P}}_0\widehat{\boldsymbol{P}}_{\mathcal{E}}\widehat{\boldsymbol{P}}_0\boldsymbol{e}_{n(k)} - 2\boldsymbol{e}_{n(k)}^T\widehat{\boldsymbol{P}}_0\widehat{\boldsymbol{P}}_{\mathcal{E}}\widehat{\boldsymbol{P}}_0\sum_{i=0}^{k-1}\boldsymbol{\phi}_i^{\pi}(\boldsymbol{\phi}_i^{\pi})^H\boldsymbol{e}_{n(k)} + \boldsymbol{e}_{n(k)}^T\widehat{\boldsymbol{P}}_0\sum_{i=0}^{k-1}\boldsymbol{\phi}_i^{\pi}(\boldsymbol{\phi}_i^{\pi})^H\widehat{\boldsymbol{P}}_{\mathcal{E}}\widehat{\boldsymbol{P}}_0\sum_{i=0}^{k-1}\boldsymbol{\phi}_i^{\pi}(\boldsymbol{\phi}_i^{\pi})^H\boldsymbol{e}_{n(k)} \quad (16)$$

in terms of SIDR introduced by spreading the interferences over all wrongly inferred null-space dimensions. Moreover, as we can see in Figure 5, this term provides the π-waveforms with robustness to subspace leakage, minimizing the impact of null-space detection errors. Comparing now (9) and (12), we have that

$$\frac{\mathrm{SIDR}_{\mathrm{SD}}^{\text{worst-case}}}{\mathrm{SIDR}_{\mathrm{DS}}^{\text{worst-case}}} = \frac{1}{N\mu\epsilon}\frac{\kappa-\epsilon}{1-\epsilon}, \quad (14)$$

which further remarks the robustness of DS schemes under the same worst-case conditions. Actually, as depicted in Figure 5 for a fixed ϵ, the average SIDR achievable by SD schemes lower-bounds the worst-case SIDR exhibited by DS.

As a final discussion, in the multi-antenna case, the autocorrelation matrix is block-Toeplitz under WSS conditions. Thus, an extension of the Szegö's Theorem for block-Toeplitz matrices [19] confirms that the derived expressions are still valid with the particularity that $N \approx TW$ should be replaced by $N \approx \eta TW$, being η the number of active or effective antennas.

V. Conclusion

This letter has studied the impact of subspace leakage on two families of null-space precoding schemes through the SIDR metric. We have derived theoretical expressions to assess the impact of different model parameters on the average and worst-case SIDR exhibited by SD and DS null-space precoding schemes. Supported by numerical results, the letter has also provided the explicit SIDR performance gain of DS in front of SD schemes as an interference mitigation strategy. The latter emphasizes the potential interest in considering DS-based null-space approaches in practical scenarios sensitive to null-space inference errors and/or with low-rate feedback requirements.

Appendix

Recalling the definition of $\widehat{\boldsymbol{P}}_k$ in Section II-B and plugging (5) into (3), note that $\boldsymbol{\phi}_k^{\pi} = \gamma_k\widehat{\boldsymbol{P}}_k\boldsymbol{e}_{n(k)}$, with $\gamma_k = (\boldsymbol{e}_{n(k)}^T\widehat{\boldsymbol{P}}_k\boldsymbol{e}_{n(k)})^{-1/2}$. Then, particularizing I_{T} in (6), I_{T}^{π} yields

$$I_{\mathrm{T}}^{\pi} = \frac{1}{N}\sum_{k=0}^{K-1}\boldsymbol{e}_{n(k)}^T\widehat{\boldsymbol{P}}_k\widehat{\boldsymbol{P}}_{\mathcal{E}}\widehat{\boldsymbol{P}}_k\boldsymbol{e}_{n(k)}\left(\boldsymbol{e}_{n(k)}^T\widehat{\boldsymbol{P}}_k\boldsymbol{e}_{n(k)}\right)^{-1}. \quad (15)$$

Using the definition of $\widehat{\boldsymbol{P}}_k$ in the numerator, it reads as in (16) on the top of the page. In the second line of (16), since $\langle\widehat{\boldsymbol{P}}_{\mathcal{E}}\rangle \subset \langle\widehat{\boldsymbol{P}}_0\rangle$ we have that $\boldsymbol{e}_{n(k)}^T\widehat{\boldsymbol{P}}_0\widehat{\boldsymbol{P}}_{\mathcal{E}}\widehat{\boldsymbol{P}}_0\boldsymbol{e}_{n(k)} = \boldsymbol{e}_{n(k)}^T\widehat{\boldsymbol{P}}_{\mathcal{E}}\boldsymbol{e}_{n(k)}$, that is, the k-th diagonal element of the projector $\widehat{\boldsymbol{P}}_{\mathcal{E}}$. The remaining terms in (16) combine off-diagonal elements of projectors $\widehat{\boldsymbol{P}}_0$ and $\widehat{\boldsymbol{P}}_{\mathcal{E}}$, constituting the second-order term δ_k. The denominator in (15) can be written as $\boldsymbol{e}_{n(k)}^T\widehat{\boldsymbol{P}}_0\boldsymbol{e}_{n(k)} - \boldsymbol{e}_{n(k)}^T\sum_{i=0}^{k-1}\boldsymbol{\phi}_i^{\pi}(\boldsymbol{\phi}_i^{\pi})^H\boldsymbol{e}_{n(k)} = \boldsymbol{e}_{n(k)}^T\widehat{\boldsymbol{P}}_0\boldsymbol{e}_{n(k)} - \xi_k$, where the first term is the k-th diagonal element of $\widehat{\boldsymbol{P}}_0$, and ξ_k is a second-order term combining off-diagonal elements of $\widehat{\boldsymbol{P}}_0$.

References

[1] W. Fu, R. Yao, F. Gao, J. C. F. Li, and M. Lei, "Robust null-space based interference avoiding scheme for d2d communication underlaying cellular networks," in *2013 IEEE Wireless Commun. and Netw. Conf. (WCNC)*, 2013, pp. 4158–4162.

[2] L. S. Cardoso, M. Kobayashi, F. R. P. Cavalcanti, and M. Debbah, "Vandermonde-subspace frequency division multiplexing for two-tiered cognitive radio networks," *IEEE Trans. Commun.*, vol. 61, no. 6, pp. 2212–2220, Jun 2013.

[3] W. Liu, Q. Feng, J. Pang, Q. Hu, R. Yin, and G. Yu, "Robust rate-maximization precoder design for VFDM system," *IEEE Trans. Veh. Technol.*, vol. 69, no. 3, pp. 2747–2757, 2020.

[4] Q. Feng, J. Pang, M. Maso, M. Debbah, and W. Tong, "IDFT-VFDM for supplementary uplink and LTE-NR co-existence," *IEEE Trans. Wireless Commun.*, vol. 19, no. 5, pp. 3435–3448, 2020.

[5] M. Maso, M. Debbah, and L. Vangelista, "A distributed approach to interference alignment in OFDM-based two-tiered networks," *IEEE Trans. Veh. Technol.*, vol. 62, no. 5, pp. 1935–1949, 2013.

[6] L. Lu, G. Y. Li, and A. Maaref, "Spatial-frequency signal alignment for opportunistic transmission," *IEEE Trans. Signal Process.*, vol. 62, no. 6, pp. 1561–1575, Mar 2014.

[7] ——, "Nullspace releasing for spatial-frequency opportunistic transmission," *IEEE Commun. Lett.*, vol. 18, no. 10, pp. 1843–1846, 2014.

[8] H. Yi, "Nullspace-based secondary joint transceiver scheme for cognitive radio MIMO networks using second-order statistics," in *2010 IEEE Int. Conf. Commun.*, 2010, pp. 1–5.

[9] S. M. Perlaza, N. Fawaz, S. Lasaulce, and M. Debbah, "From spectrum pooling to space pooling: opportunistic interference alignment in MIMO cognitive networks," *IEEE Trans. Signal Process.*, vol. 58, no. 7, pp. 3728–3741, Jul 2010.

[10] C. G. Tsinos and K. Berberidis, "Blind opportunistic interference alignment in MIMO cognitive radio systems," *IEEE J. Emerging Sel. Topics in Circuits and Systems*, vol. 3, no. 4, pp. 626–639, 2013.

[11] M. El-Absi, M. Shaat, F. Bader, and T. Kaiser, "Interference alignment with frequency-clustering for efficient resource allocation in cognitive radio networks," *IEEE Trans. Wireless Commun.*, vol. 14, no. 12, pp. 7070–7082, 2015.

[12] L. Lu, G. Y. Li, A. Maaref, and R. Yao, "Opportunistic transmission exploiting frequency- and spatial-domain degrees of freedom," *IEEE Wireless Commun.*, vol. 21, no. 2, pp. 91–97, April 2014.

[13] M. Shaghaghi and S. A. Vorobyov, "Subspace leakage analysis and improved DOA estimation with small sample size," *IEEE Trans. Signal Process.*, vol. 63, no. 12, pp. 3251–3265, 2015.

[14] J. Borras and G. Vazquez, "Interference mitigation in feedforward opportunistic communications," *IEEE Trans. Commun.*, vol. 71, no. 5, pp. 2977–2991, 2023.

[15] Z. Chen, C.-X. Wang, X. Hong, J. Thompson, S. A. Vorobyov, F. Zhao, and X. Ge, "Interference mitigation for cognitive radio mimo systems based on practical precoding," *Phys. Commun.*, vol. 9, pp. 308–315, 2013.

[16] D. Tse and P. Viswanath, *Fundamentals of Wireless Communication*. Cambridge University Press, 2005.

[17] M. Benzi and V. Simoncini (eds.), *Exploiting hidden structure in matrix computations: Algorithms and applications*. Springer, 2016.

[18] R. M. Gray, "Toeplitz and circulant matrices: A review," *Foundations and Trends® in Communications and Information Theory*, vol. 2, no. 3, pp. 155–239, 2006.

[19] D. Ramirez, G. Vazquez-Vilar, R. Lopez-Valcarce, J. Via, and I. Santamaria, "Detection of rank- p signals in cognitive radio networks with uncalibrated multiple antennas," *IEEE Trans. Signal Process.*, vol. 59, no. 8, pp. 3764–3774, 2011.